Resonance Investigation and Active Damping Method for VSC-HVDC Transmission Systems under Unbalanced Faults

Xin Tang[*], Ruoshui Zhan[*], Yanhui Xi[†], and Xianyong Xu[*]

[†,*]School of Electrical and Information Engineering,
Changsha University of Science and Technology, Changsha, China

Abstract

Grid unbalanced faults can cause core saturation of power transformer and produce lower-order harmonics. These issues increase the electrical stress of power electronic devices and can cause a tripping of an entire HVDC system. In this paper, based on the positive-sequence and negative-sequence impedance model of a VSC-HVDC system as seen from the point of common connection (PCC), the resonance problem is analyzed and the factors determining the resonant frequency are obtained. Furthermore, to suppress over-voltage and over-current during resonance, a novel method using a virtual harmonic resistor is proposed. The virtual harmonic resistor emulates the role of a resistor connected in series with the commutating inductor without influencing the active and reactive power control. Simulation results in PSCAD/EMTDC show that the proposed control strategy can suppress resonant over-voltage and over-current. In addition, it can be seen that the proposed strategy improves the safety of the VSC-HVDC system under unbalanced faults.

Key words: Core saturation, High voltage direct current, Impedance frequency characteristics, Resonance, Unbalanced fault, Virtual harmonic resistor, Voltage-source converter

I. INTRODUCTION

High-voltage direct current (HVDC) transmission with voltage-source converters (VSCs), namely VSC-HVDC, is a new and developing technology. It uses state of the art insulated-gate bipolar transistor (IGBT) technology and pulse width modulation (PWM) with relatively high switching frequencies to generate desired waveforms. VSC-HVDC has a number of potential merits. For instance, it can independently control active and reactive power [1]. As a result, a VSC-HVDC system has broad applications in the connection of new renewable energy power plants (such as wind farms and solar power) to a main grid, as well as feeding remote and isolate loads, building urban DC power distribution networks, etc. [2].

The operation of VSC-HVDC has a lot of advantages including constant DC voltage, lower harmonic distortion and sinusoidal AC voltage under normal conditions. However, unbalanced faults can occur from time to time, which deteriorates the DC bias problem of converter transformers and makes transformers produce a large number of low-order harmonics [3]. These harmonics interact with switching functions and result in the generation of greater non-characteristic harmonics on both side of the converter [4], [5]. Moreover, it is possible to cause over-voltage and over-current, which can influence the safe operation of the system due to resonance [6]. The phenomenon of resonance has appeared in line-commutated converter HVDC (LCC-HVDC) systems and STATCOMs based power electronic devices [7].

A characteristic double frequency ripple occurs on the DC voltage under AC grid unbalanced conditions in VSC-HVDC systems. This phenomenon is deteriorated under single-phase grounding faults [8]. In order to restrain power fluctuations and to eliminate harmonics, a negative-sequence voltage was

introduced to the output voltage control of the VSC [9]. To improve the transient performances, two decoupled and independently controllable subsystems including positive and negative sequence subsystems were built [10]. Recently, a whole controller has been implemented in the stationary frame for deriving a special current reference generator to avoid the low bandwidth of the current regulator due to sequence extraction [11], [12]. The above methods suppress the second harmonic power ripple caused by the fundamental negative-sequence voltages and currents at the AC side of VSC-HVDC systems. However, these methods cannot be extended to analyze and solve the problem of resonance between the AC grid and the VSC-HVDC system at low-order harmonics frequency under unbalanced faults. Therefore, "harmonic transfer through converters" in a VSC has been analyzed and a combination dc voltage decoupling with an ac current-tracking control strategy has been proposed, which can effectively eliminate the harmonic transfer from the DC side to the AC side of converters [5].

The equivalent impedance of a VSC-HVDC system as seen from the point of common connection (PCC) may be capacitive at a low-order harmonic frequency. Thus, resonance between the VSC-HVDC system and the AC grid can occur easily and can amplify the harmonics produced by the converter transformer [5], [13]. The short-circuit ratio (SCR) of an AC grid connected to a VSC-HVDC system has already been shown to be a key factor in maximum power transmission [14]. In addition, power-synchronization control for grid-connected VSCs has been shown to be good solution for VSC-HVDC systems connected to a weak AC grid [15]. However, the SCR effects on the resonant frequency between a VSC-HVDC system and an AC grid are not involved. The influence of capacitors on the low resonant frequency of a two-level VSC–HVDC is analyzed in [16] using the impedance modelling method. However, the damping control method to suppress the resonances is not given. The additional resistor is a solution to prevent the resonance. However, it significantly increases the power loss in the system. Therefore, the active damping technique, which is equivalent to introducing a virtual resistor, is more suitable for mitigating the resonance and for maintaining a high efficiency. A damping control for a wind power plant connected to a two-level VSC- based DC grid was proposed in [17]. The active damping technique was also applied in VSCs to mitigate the resonance and to maintain a high efficiency [18]-[21]. However, the virtual resistor degrades the dynamic performance. In this paper, the impacts of the SCR and DC side capacitor of a VSC-HVDC system on the resonant characteristics of a network is analyzed. Then, a virtual harmonic resistor, which is similar to the proposed active resistance, is proposed to suppress resonant over-voltage and over-current. The virtual harmonic resistor emulates the role of a resistor connected in series with the commutating inductor. However, unlike the conversional

damping method, it has no influence on the dynamic performance of active and reactive power control.

The remainder of this paper is structured as follows. Section II describes an impedance model of a VSC-HVDC system in a low-frequency band. A virtual harmonic resistor is presented in Section III. In addition, an inner current controller and the principle of the virtual harmonic resistor are described. Section IV describes and briefly analyzes the results of simulations based on PSCAD/EMTDC. The conclusion of the paper is presented in Section V.

II. IMPEDANCE FREQUENCY OF A VSC-HVDC SYSTEM

A. Brief Description of a VSC-HVDC System

A general schematic of a VSC-HVDC system is shown in Fig. 1. The converters consist of three-phase, two-level, six-pulse bridges with IGBTs using sinusoidal PWM. The converter stations are connected to the AC grid through transformers. The inverter station is connected to the rectifier station through a DC transmission line. Z_s is the equivalent impedance of the AC system and $R+j\omega L$ is the impedance of the commutating inductor. Filters are used to eliminate the high frequency switching harmonics. Transformers provide suitable voltages for the VSCs, and DC side capacitors are used to minimize the DC voltage ripple.

B. Impedance Model for a VSC-HVDC System

The relationship between the DC voltage and the AC voltages, neglecting the switching harmonic components of the VSC with sinusoidal PWM, can be expressed as [5], [13]:

$$u_{ck} = 0.5u_{dc}S_{uk}(k = a,b,c) \tag{1}$$

where u_{dc} is the voltage across the DC bus, u_{ck} (k=a, b, c) are the voltages at AC side of the converter station, and S_{uk} (k=a,b,c) are the switching functions:

$$S_{ua} = M\sin(\omega_0 t + \delta) \tag{2}$$

$$S_{ub} = M\sin(\omega_0 t + \delta - 120^0) \tag{3}$$

$$S_{uc} = M\sin(\omega_0 t + \delta + 120^0) \tag{4}$$

where M is the modulating coefficient, δ is the phase angle, and ω_0 is the angular frequency of the AC supply, respectively.

The relationship between the DC current and the AC currents can be expressed as:

$$i_{dc} = i_a S_{ia} + i_b S_{ic} + i_c S_{ic} \tag{5}$$

where i_{dc} is the current in the DC bus, i_k (k=a, b, c) are the currents in the commutating inductor, and S_{ik} (k=a,b,c) are the switching functions taking the form:

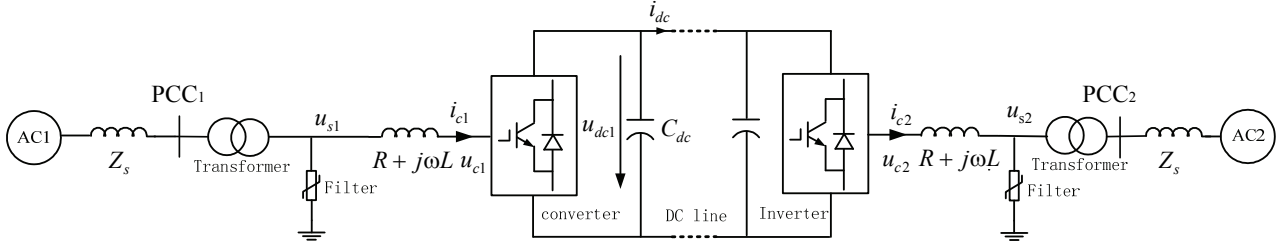$$S_{ia} = 0.5 + 0.5M\sin(\omega_0 t + \delta) \tag{6}$$

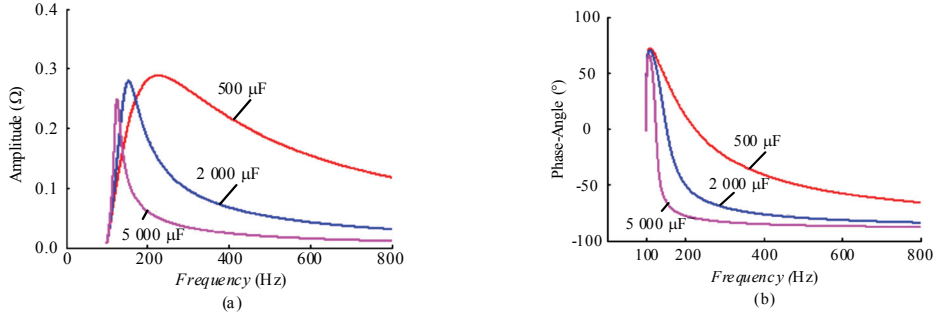Fig. 1. Schematic diagram of a VSC-HVDC system.

Fig. 2. Frequency characteristic of the positive-sequence impedance. (a) Amplitude-frequency characteristics. (b) Phase-frequency characteristics.
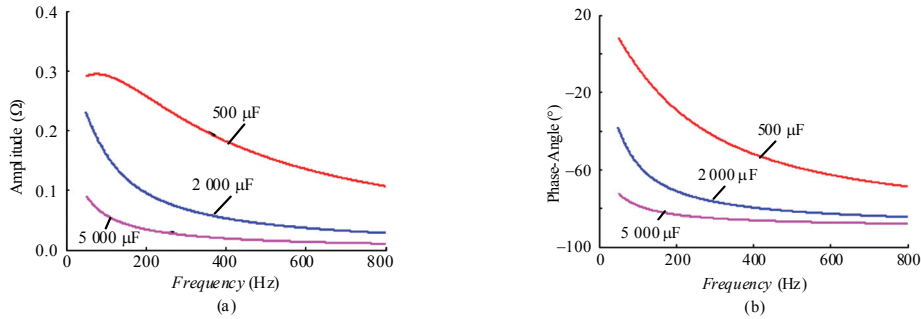

Fig. 3. Frequency characteristic of the negative-sequence impedance. (a) Amplitude-frequency characteristics. (b) Phase-frequency characteristics.

$$S_{ib} = 0.5 + 0.5M \sin\left(\omega_0 t + \delta - 120^0\right) \tag{7}$$

$$S_{ic} = 0.5 + 0.5M \sin\left(\omega_0 t + \delta + 120^0\right) \tag{8}$$

Assuming that a positive-sequence harmonic, where the angular frequency ω ($\omega \neq \omega_0$), is introduced on the AC side of the converter, according to the law of harmonic transferring through converters [13], the positive-sequence and negative-sequence impedance of the VSC-HVDC system from the PCC view can be computed by [5]:

$$\begin{cases} Z_{ac}^+(\omega) = \dfrac{3}{16} \dfrac{M^2}{m\angle\lambda} Z_{dc}(\omega - \omega_0) \\ m\angle\lambda = 1 + \dfrac{3}{16} M^2 \dfrac{Z_{dc}(\omega - \omega_0)}{Z_{ac}^-(\omega - 2\omega_0)} \end{cases} \tag{9}$$

$$\begin{cases} Z_{ac}^-(\omega) = \dfrac{3}{16} \dfrac{M^2}{m\angle\lambda} Z_{dc}(\omega + \omega_0) \\ m\angle\lambda = 1 + \dfrac{3}{16} M^2 \dfrac{Z_{dc}(\omega + \omega_0)}{Z_{ac}(\omega + 2\omega_0)} \end{cases} \tag{10}$$

where ω_0 is the angular frequency of the AC supply, M is the modulating coefficient, λ is the angle of the impedance, $Z_{ac}^+(\omega)$ is the positive-sequence impedance of the VSC-HVDC system as seen from the PCC, $Z_{ac}^-(\omega)$ is the negative-sequence impedance of the VSC-HVDC system as seen from the PCC, and Z_{dc} is the impedance on the DC side as seen across the DC bar.

C. Influence of DC Capacitors on the Network Resonant Frequency

As described above, DC side capacitors have an effect on the AC impedance of VSC-HVDC systems. Fig. 2 and Fig. 3 show the frequency characteristic of the positive-sequence and negative-sequence input impedance $Z_{ac}(\omega)$ with the following parameters: $M = 0.8$, $R_{dc} = 1\Omega$, $L_{dc} = 15.9mH$, $R_{ac} = 0.0071\Omega$ and $L_{ac} = 0.675mH$. As shown in Fig. 2 and Fig. 3, the positive-sequence and negative-sequence impedance of the converter station may be capacitive in the frequency
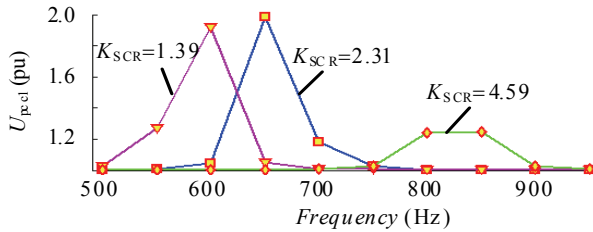
Fig. 4. Network resonant frequency under different SCRs.

band of the characteristic harmonics produced by converter transformers. Furthermore, it is found that the impedance $Z_{ac}(\omega)$ becomes capacitive at a lower frequency with an increase of the DC side capacitance. In comparison with grid-connected converters, the DC side capacitance of converter stations is much bigger. Thus, it is easier for network resonance to take place at a low-order harmonic frequency. In addition, it can amplify the characteristic harmonics of converter transformers and the non- characteristic harmonics under unbalanced faults.

D. Influence of the SCR of an AC Grid on Network Resonant Frequency

The strength of an AC grid connected to a VSC-HVDC system is mainly depended on the equivalent impedance of the grid [22], which can be described using the short circuit ratio (SCR). The SCR is written as [15], [23]:

$$\text{SCR} = \frac{U_{acN}^2}{P_{dcN}} \frac{1}{|Z_s|} \tag{11}$$

where U_{acN} is the rating voltage of the ac grid, P_{dcN} is the rating power at the dc side, and Z_s represents the equivalent impedance of the AC grid as seen from the PCC.

When the SCR is lower than 3.0, the grid is considered to be a weak system, otherwise it is strong. The network resonant frequency under different SCRs is shown in Fig. 4. A current harmonic source with a magnitude of 0.1pu and a different frequency at the PCC1 produces a corresponding harmonic voltage with a different magnitude due to network resonance. It can be seen that the resonant frequency is also different under different SCRs (SCR=1.39, 2.31, 4.59). Moreover, with a decrease of the SCR, the resonant frequency decreases accordingly. That is to say, a weak AC grid makes it easier to achiever resonance between a VSC-HVDC system and an ac grid at the characteristic harmonic frequency of the converter transformers.

III. PRINCIPLE OF VIRTUAL HARMONIC RESISTORS

The conventional method for restraining the network resonance is to regulate the system parameters to avoid resonance at a certain frequency. However, taking care of one often results in losing others. To suppress resonant over-voltage and over-current, an additional algorithm is proposed,

which simulates the role of a resistor connected in series with a commutating inductor without affecting the active and reactive power control.

The control system of a VSC-HVDC system is a cascade control system, which consists of an inner loop and an outer loop. The inner controller is referred to as the current controller, and the outer controllers, which supply the current references for the inner controller, use a reactive power controller and a DC voltage controller for the rectifier station, and a reactive power controller and an active power controller for the inverter station [24], [25].

A. The Inner Current Controller

All of the quantities of the rectifier station are implemented in the synchronously rotating coordinate frame. The converter station output voltages in the d-q coordinate frame are as follows:

$$u_{c1d} = -L\frac{di_{c1d}}{dt} - Ri_{c1d} - \omega Li_{c1q} + u_{s1d} \tag{12}$$

$$u_{c1q} = -L\frac{di_{c1q}}{dt} - Ri_{c1q} + \omega Li_{c1d} + u_{s1q} \tag{13}$$

where ω is the system angular frequency; u_{c1d}, u_{c1q}, u_{s1d}, u_{s1d}, i_{c1d} and i_{c1q} are the d-q components of the converter output voltages, the voltages at PCC1, and the current through the commutating inductor, respectively. This paper only analyzes the rectifier station since the principle is same for the inverter station. Fig. 5 shows the structure of the inner current controller.

B. The Virtual Harmonic Resistor

If a resistor is connected in series with the commutating inductor, the over-voltage and over-current arising from the network resonance can be restrained. However, the introduced resistor results in power loss. In this paper, a novel method to restrain resonant over-voltage and over-current is proposed. The proposed virtual harmonic resistor is shown in Fig. 6, and R_{v_h} is the coefficient. Based on instantaneous reactive power theory [26], [27], the fundamental components of grid currents i_{c1d_f} and i_{c1q_f} can be obtained using low pass filters (LPFs). Then, the harmonics components of the grid currents i_{c1d_h} and i_{c1q_h} are equal to the fundamental component minus the grid currents. If the LPFs are well designed, the virtual harmonic resistor barely affects the active and reactive power control. When the delay of the calculation and switching is neglected, Fig. 7(a) and (b) show equivalent circuits of Fig. 6 when only considering the fundamental component and the harmonics component, respectively. Fig. 7(b) can be further transformed into Fig. 7(c). It can be seen that the virtual harmonic resistor emulates the roles of a resistor but only works for harmonics. It is equivalently connected in series with the commutating inductor of the converter stations. Thus, the resonant
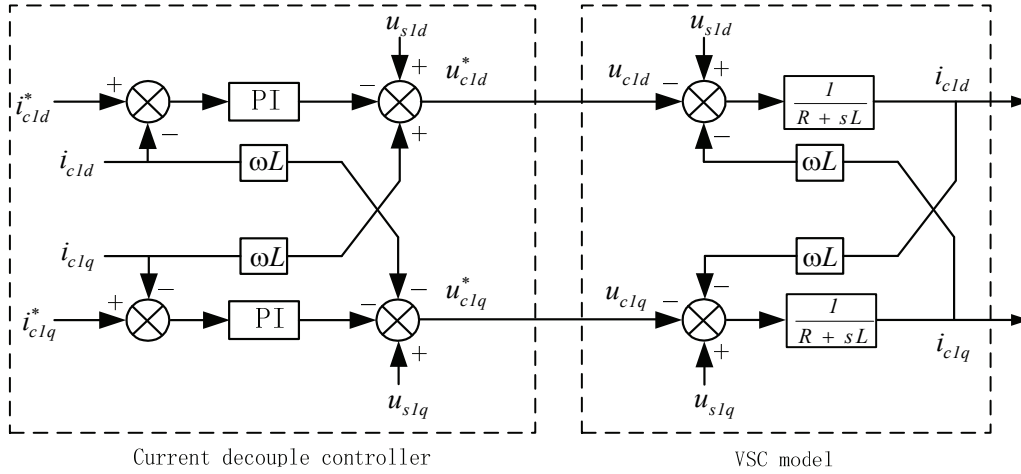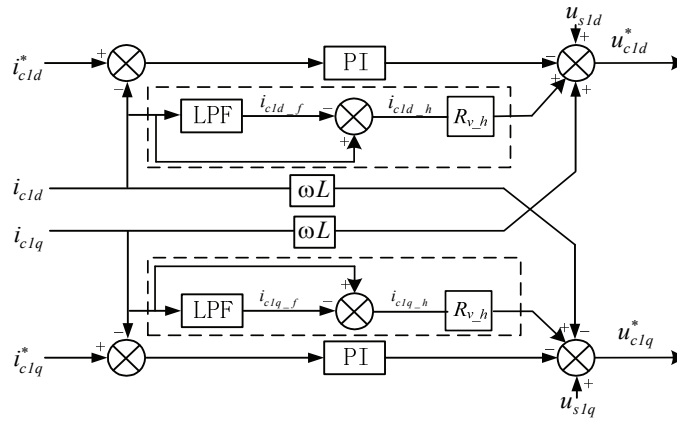
Fig. 5. Inner current controller.

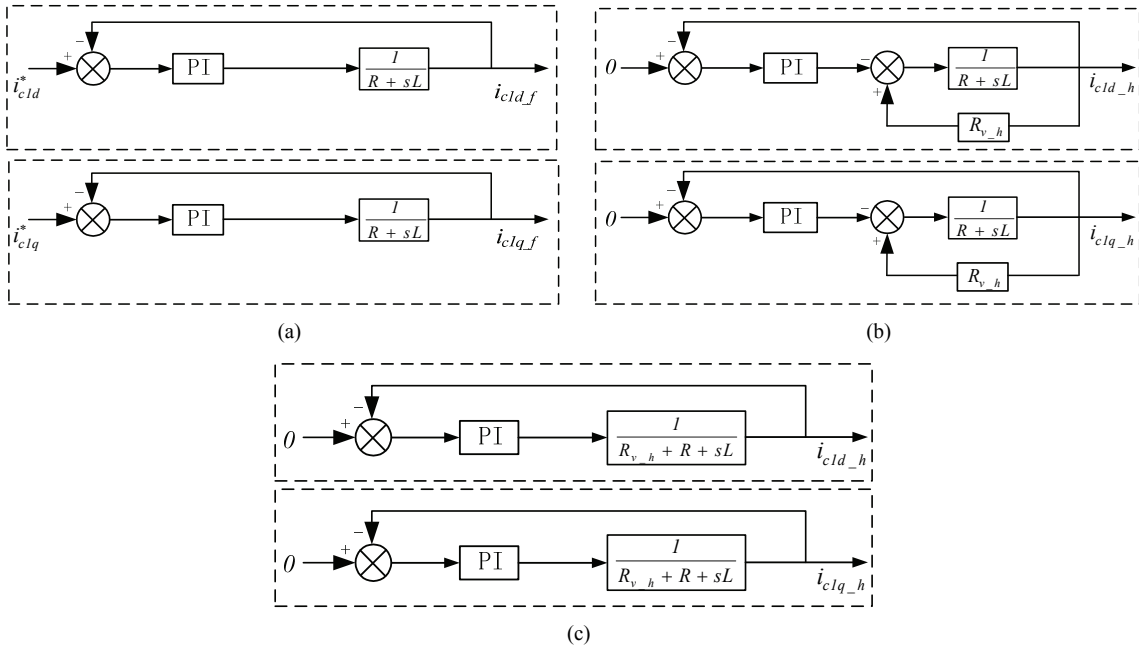Fig. 6. Current controller with a virtual harmonic resistor.

Fig. 7. Equivalent circuits of Fig. 6. (a) Only considering the fundamental component. (b) Only considering the harmonic component. (c) Equivalent circuit of Fig. 6 (b).
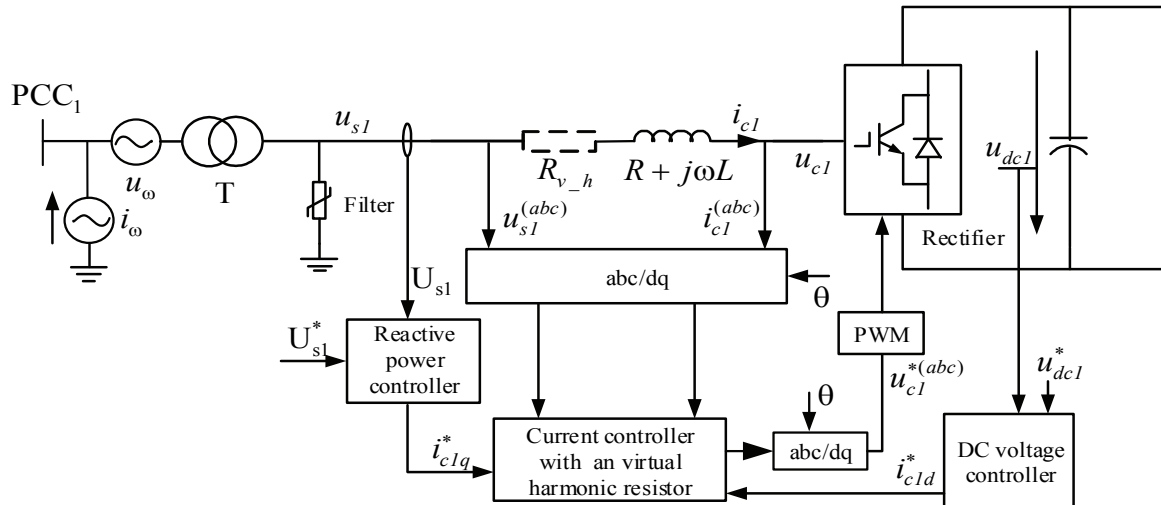
Fig. 8. Control system of the rectifier station of a VSC-HVDC system.

overvoltage and over current can be suppressed.

The whole control system of the rectifier station is shown in Fig. 8, where i_ω and u_ω are the current and voltage harmonic sources, which emulate the harmonics produced by the converter transformer.

C. Design of the Virtual Harmonic Resistor

After the virtual harmonic resistor is introduced, the circuit can be considered to be an LCR circuit with a damping ratio:

$$\zeta = \frac{R_{v\_h}}{2}\sqrt{\frac{C_{eq}}{L_{eq}}} \tag{14}$$

Where C_{eq} is the equivalent capacitance of the VSC-HVDC system as seen from the PCC, and L_{eq} is the equivalent inductance of the ac grid as seen from the PCC. Thus, the value of the virtual harmonic resistor can be determined by the damping requirements and system parameters. To suppress the over-voltage and over-current, the damping ratio ξ is set to 1.

IV. SIMULATION RESULTS

To verify the validity and feasibility of the proposed control strategy, the model of the VSC-HVDC system shown in Fig. 1 is built and simulated in PSCAD/EMTD.

In the following cases studies, the proposed control method is used for both of the converter stations of the VSC-HVDC system shown in Fig. 8. In addition, the parameters of the VSC-HVDC system are shown in Table I [28]. The resonant frequency between the AC grid and the VSC-HVDC system is around 580Hz according to (9) and (10). The virtual harmonic resistor R_{v_h} is set to 3Ω.

Core saturation of the transformer causes a significant increase of the characteristic harmonics and non-characteristic harmonics under unbalanced faults. To simplify the analysis,

TABLE I
SYSTEM PARAMETERS

S_{sys}	Rated apparent power	12.235MVA
U_{ac1}	Rated AC1 voltage	10.7 kV
U_{pcc1}	Rated PCC$_1$ voltage	4.16 kV
U_{ac2}	Rated AC2 voltage	4.16 kV
U_{dc}	Dc voltage	10 kV
Z_s	System equivalent impedance	0.0071+j1.036 Ω
SCR	Short circuit ratio	1.39
R_{v_h}	Virtual harmonic resistor	3 Ω
$R+j\ L$	Phase impedance	0.0071+j0.212 Ω
C_{dc}	Dc capacitor	5600 μF
f	Grid frequency	50 Hz

this paper emulates the low-order harmonics arising from the transformer by using the current and voltage harmonic source under unbalanced faults shown in Fig. 8 [29].

A. Current Harmonics as Sources

A set of current harmonic sources of 550Hz, 600Hz and 650Hz, each having a magnitude of 0.1pu, emulate the current harmonics arising from the converter transformer under unbalanced faults. Those harmonics are injected into the ac bus (PCC1) at 3s and are cleared after 0.2s. Fig. 9 shows the performance of a VSC-HVDC system with and without a virtual harmonic resistor when there are current harmonics as sources. Tables II and III show the harmonic distortion (HD) of the currents and voltages, respectively. As can be seen, before the virtual harmonic resistor is implemented, the parallel resonance between the AC grid and the VSC-HVDC system results in very high magnitudes of 11th, 12th and 13th harmonic voltages at PCC1 when there are the corresponding current harmonics. Total harmonic distortion (THDv%) of the a-phase voltage at PCC1 u_{pcc1a} was greater than 1, which results in the total harmonic distortion (THDi%) of the a-phase current in the commutating
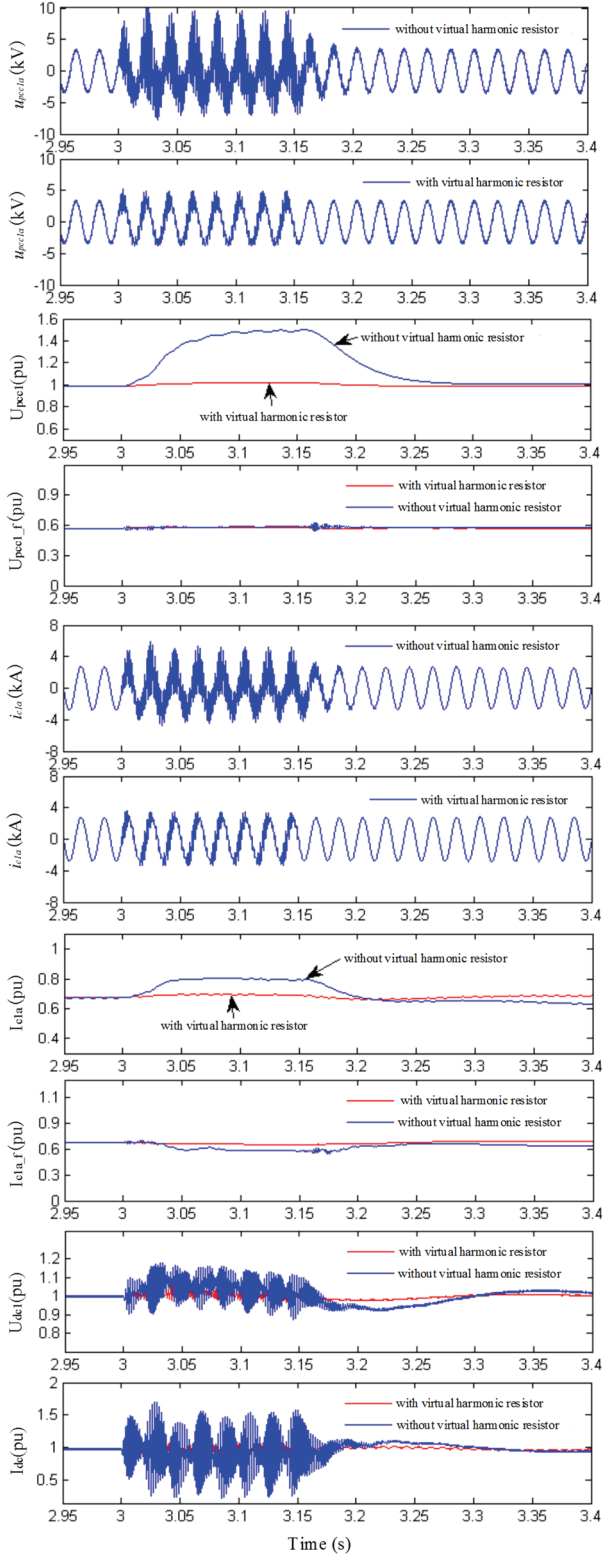
Fig. 9. Performance of a VSC-HVDC system with and without a virtual harmonic resistor when there are current harmonics as sources (from top to bottom: a-phase voltage at PCC1, RMS of the a-phase voltage and fundamental voltage at PCC1, a-phase current in the commutating inductor, RMS of the a-phase current and fundamental current in the commutating inductor, dc voltage, dc current).

TABLE II
VOLTAGE DISTORTION OF THE HARMONICS IN FIG. 9

Control method	HD_{11}/%	HD_{12}/%	HD_{13}/%	THD_v/%
Without virtual harmonic resistor	57.21	104.13	31.73	123.01
With virtual harmonic resistor	25.55	18.93	14.61	35.02

TABLE III
CURRENT DISTORTION OF THE HARMONICS IN FIG. 9

Control method	HD_{11}/%	HD_{12}/%	HD_{13}/%	THD_v/%
Without virtual harmonic resistor	33.34	81.62	30.47	93.81
With virtual harmonic resistor	23.82	19.61	16.75	35.11

TABLE IV
VOLTAGE DISTORTION OF THE HARMONICS IN FIG. 10

Control method	HD_{11}/%	HD_{12}/%	HD_{13}/%	THD_v/%
Without virtual harmonic resistor	43.56	54.30	20.94	78.18
With virtual harmonic resistor	10.20	2.73	4.53	12.34

TABLE V
CURRENT DISTORTION OF THE HARMONICS IN FIG. 10

Control method	HD_{11}/%	HD_{12}/%	HD_{13}/%	THD_v/%
Without virtual harmonic resistor	86.87	95.82	31.39	141.05
With virtual harmonic resistor	16.42	7.89	10.46	21.35

inductor i_{pc1a} reaching up to 98.5%. Hence, the RMS of u_{pcc1a} increased to 1.51pu, and the RMS of i_{c1a} increased from 0.67pu to 0.80pu. In addition, there were also greater voltage and current fluctuation on the dc-side of the VSC-HVDC system. After the virtual harmonic resistor was introduced, the THD_v% of u_{pcc1a} and THD_i% of i_{c1a} were reduced to 35.11% and 35.31%, respectively. The RMS of u_{pcc1a} merely increased to 1.02pu, and the RMS of i_{c1a} barely increased. The fluctuations of the dc voltage and the dc current were also mitigated. It is worth mentioning that the performance of the VSC-HVDC system with the virtual harmonic resistor is similar that without the virtual harmonic resistor under normal conditions. This means that the virtual harmonic resistor does not influence active and reactive power control.

B. Voltage Harmonics as Sources

In this simulation, a set of voltage harmonics sources of 550Hz, 600Hz and 650Hz, each having a of 0.04pu, are injected into the ac bus (PCC1) at 3s and are cleared after 0.2s. Fig. 10 shows the performance of the VSC-HVDC system with and without a virtual harmonic resistor when there are voltage harmonics as sources. Tables IV and V show the HD of currents and voltages, respectively. As can be seen, before the virtual harmonic resistor is implemented, the series resonance between a finite ac grid and the VSC-HVDC system caused very high magnitudes of 11th, 12th and 13th harmonic currents when there were corresponding voltage harmonics. The THD_i% of the a-phase current in the commutating inductor i_{c1a} reached up to 78.18%,
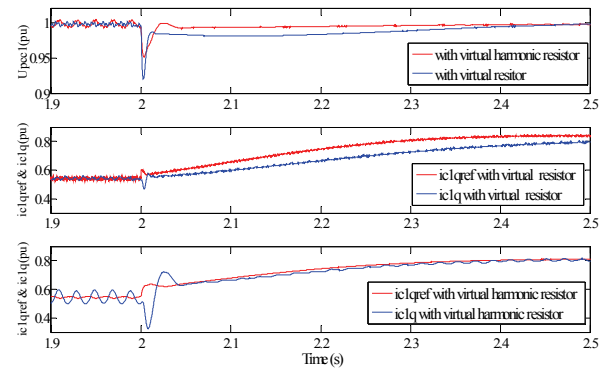
Fig. 11. the dynamic performance of the rectifier station with a virtual harmonic resistor and with a virtual resistor (from top to bottom: RMS of the voltage at PCC1, reactive current and the reference of the rectifier station with a virtual resistor, reactive current and the reference of the rectifier station with a virtual harmonic resistor).

which results in a THDv% of the a-phase voltage at PCC1 u_{pcc1a} that is greater than 1. Therefore, the RMS of u_{pcc1a} increased to 1.52pu, and the RMS of i_{c1a} increased from 0.67pu to 0.95pu. In addition, there were also greater voltage and current fluctuation on the dc side of the converter station. After the virtual harmonic resistor was introduced, the THDi% of u_{pcc1a} and THDv% of i_{c1a} were reduced to 12.34% and 21.35%, respectively. Both the RMS of u_{pcc1a} and the RMS of i_{c1a} barely changed. The fluctuations of the dc voltage and dc current were greatly reduced. Similar to Case A, the proposed strategy can suppress the over-voltage and over current caused by series resonance without influencing the active and reactive power control.

C. Dynamic Performance

In this simulation, dynamic performances of the rectifier station with a virtual harmonic resistor and with a virtual resistor are compared, as shown in Fig. 11, when a resistive load is applied at PCC1 at 2s. As can be seen, the rectifier station with a constant ac voltage control produces reactive current to stabilize the voltage at PCC1 when a load is switched. The RMS of u_{pcc1} drops to about 0.92pu because the reactive current cannot tightly track the reactive current reference when the virtual resistor is implemented. The RMS of u_{pcc1} drops to about 0.95pu since the reactive current can tightly track the reactive current reference when the virtual harmonic resistor is implemented. This means that the rectifier station with a virtual harmonic resistor has better dynamic performance.

V. CONCLUSION

In this paper, both the resonance problem and active damping method of a VSC-HVDC system are discussed. The impedance of a VSC-HVDC system as seen from the PCC may be capacitive at the frequencies of the characteristic
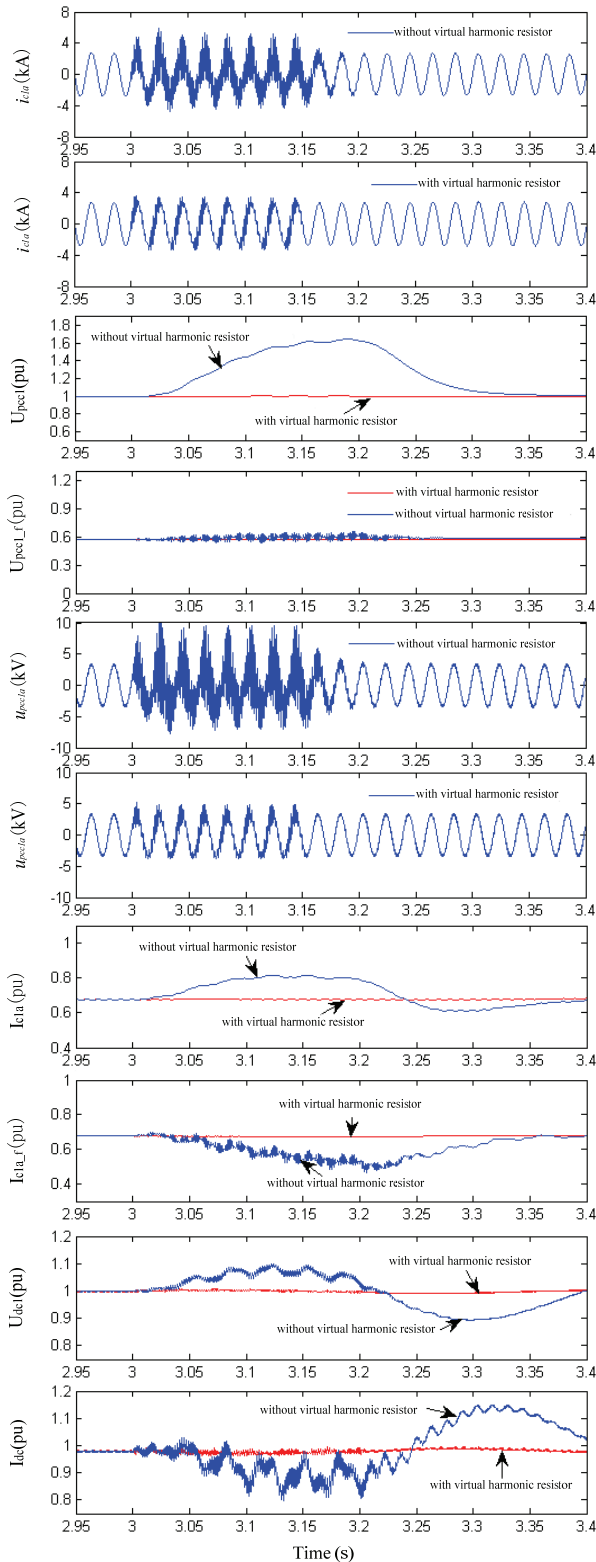

Fig. 10. Performance of a VSC-HVDC system with and without a virtual harmonic resistor when there are voltage harmonics as sources (from top to bottom: a-phase voltage at PCC1, RMS of the a-phase voltage and fundamental voltage at PCC1, a-phase current in the commutating inductor, RMS of the a-phase current and fundamental current in the commutating inductor, dc voltage, dc current).

harmonics arising from converter transformers. Therefore, the harmonics are amplified by resonance between the AC grid and the VSC-HVDC system. This issue increases the electrical stress on power devices and gets worst under unbalanced fault since grid faults make the converter transformer produce more low-order harmonics. In addition, the resonant frequency decreases with an increase of the SCR or DC side capacitance. This means that the weaker the AC grid connection to the VSC-HVDC system, the lower resonant frequency. The DC side capacitance of a VSC-HVDC system is much larger than that of a grid-connected converter which results in a lower resonant frequency.

The proposed virtual harmonic resistor emulates the roles of a resistor. However, it only works for harmonics. In addition, it is connected in series with the commutating inductor. Thus, the over-voltage and over-current caused by the resonance between the AC grid and the VSC-HVDC system can be suppressed without affecting the active and reactive power control. A rectifier station with a virtual harmonic resistor has better dynamic performance. Moreover, it does not cause any power loss.

REFERENCES

[1] M. Raza, E. P. Araujo, and O. G. Bellmunt, "Small-signal stability analysis of offshore AC network having multiple VSC-HVDC systems," *IEEE Trans. Power Del.*, Vol. 33, No. 2, pp. 830-839, Apr. 2018.

[2] M. Z. Sujod, I. Erlich, and S. Engelhardt, "Improving the reactive power capability of the DFIG-based wind turbine during operation around the synchronous speed," *IEEE Trans. Energy Convers.*, Vol. 28, No. 3, pp. 736-745, Sep. 2013.

[3] T. Augustin, I. Jahn, S. Norrga, and H. Nee, "Transient behaviour of VSC-HVDC links with DC breakers under faults," *19th European Conference on Power Electronics and Applications,* pp. 1-10, 2017.

[4] C. F. Nascimento, E. H. Watanabe and O. Diene, A. B. Dietrich, A. Goedtel, J. J. C. Gyselinck, and R. F. S. Dias, "Analysis of non-characteristic harmonics generated by voltage-source converters operating under unbalanced voltage," *IEEE Trans. Power Del.*, Vol. 32, No. 2, pp. 951-961, Apr. 2017.

[5] V. Kůs, Z. Peroutka, and P. Drábek, "Non-characteristic harmonics and interharmonics of power electronic converters," *CIRED 18th International Conference and Exhibition on Electricity Distribution,* pp. 1-5, 2005.

[6] F. Mura, C. Meyer, and R. W. De Doncker, "Stability analysis of high-power DC grids," *IEEE Trans. Ind. Appl.*, Vol. 46, No. 2, pp. 584-592, Mar./Apr. 2010.

[7] D. Shen, Z. Wang, J. Y. Chen, and Y. H. Song, "Harmonic resonance phenomena in STATCOM and relationship to parameters selection of passive components," *IEEE Trans. Power Del.*, Vol. 16, No. 1, pp. 46-52, Jan. 2001.

[8] P. N. Enjeti and S. A. Choudhury, "A new control strategy to improve the performance of a PWM AC to DC converter under unbalanced operating conditions," *IEEE Trans. Power Electron.*, Vol. 8, No. 4, pp. 493-500, Oct. 1993.

[9] G. Zhang, Z. Xu, and G. Wang, "Control strategy for unsymmetrical operation of HVDC-VSC based on the improved instantaneous reactive power theory," *Seventh International Conference on AC-DC Power Transmission*, pp. 262-267, 2001.

[10] H. S. Song and K. Nam, "Dual current control scheme for PWM converter under unbalanced input voltage conditions," *IEEE Trans. Ind. Electron.*, Vol. 46, No. 5, pp. 953-959, Oct. 1999.

[11] J. Hu and Y. He, "Modelling and control of grid-connected voltage-sourced converters under generalized unbalanced operation conditions," *IEEE Trans. Energy Convers.*, Vol. 23, No. 3, pp. 903-913, Sep. 2008.

[12] D. Roiu, R. I. Bojoi, L. R. Limongi, and A. Tenconi, "New stationary frame control scheme for three-phase PWM rectifiers under unbalanced voltage dips conditions," *IEEE Trans. Ind. Appl.*, Vol. 46, No. 1, pp. 268-277, Jan./Feb. 2010.

[13] M. Durrant, H. Werner, and K. Abbott, "Model of a VSC HVDC terminal attached to a weak AC system," *Proceedings of 2003 IEEE Conference on Control Applications,* pp. 178-182, 2003.

[14] L. Zhang, L. Harnefors, and H. Nee, "Interconnection of two very weak AC systems by VSC-HVDC links using power-synchronization control," *IEEE Trans. Power Syst.*, Vol. 26, No. 1, pp. 344-355, Feb. 2011.

[15] L. Tang and B. T. Ooi, "Converter nonintegral harmonics from AC network resonating with DC network," *Conference Record of the 2001 IEEE Industry Applications Conference*, pp. 2186-2192, 2001.

[16] L. Xu, L. Fan, and Z. Miao, "DC impedance-model-based resonance analysis of a VSC–HVDC system," *IEEE Trans. Power Del*, Vol. 30, No. 3, pp. 1221-1230, Jun. 2015.

[17] X. Wan, Y. Li, and M. Peng, "Modelling, analysis and virtual parallel resistor damping control of VSC-based DC grid using master–slave control mode," *IET Gener. Transm. Dis.*, Vol. 12, No. 9, pp. 2046-2054, Jan. 2018.

[18] R. Guzman, L. G. Vicuña, J. Morales, M. Castilla, and J. Miret, "Model-based active damping control for three-phase voltage source inverters with LCL filter," *IEEE Trans. Power Electron.*, Vol. 32, No. 7, pp. 5637-5650, Jul. 2017.

[19] H. Chen, P. Cheng, X. Wang, and F. Blaabjerg, "A passivity-based stability analysis of the active damping technique in the offshore wind farm applications," *IEEE Trans. Ind. Appl.*, Vol. 54, No. 5, pp. 5074-5082, Sep./Oct. 2018.

[20] P. A. Dahono, Y. R. Bahar, Y. Sato, and T. Kataoka, "Damping of transient oscillations on the output LC filter of PWM inverters by using a virtual resistor," *4th IEEE International Conference on Power Electronics and Drive Systems,* pp. 403-407, 2001.

[21] R. Errouissi and A. Al-Durra, "Design of PI controller together with active damping for grid-tied LCL-filter systems using disturbance-observer-based control approach," *IEEE Trans. Ind. Appl.*, Vol. 54, No. 4, pp. 3820-3831, Jul./Aug. 2018.

[22] *IEEE Guide for Planning DC Links Terminating at AC*

Locations Having Low Short-Circuit Capacities," IEEE Std 1204-1997, pp. 1-216, Jan. 1997.

[23] O. B. Nayak, A. M. Gole, D. G. Chapman, and J. B. Davies, "Dynamic performance of static and synchronous compensators at an HVDC inverter bus in a very weak AC system," *IEEE Trans. Power Syst.*, Vol. 9, No. 3, pp. 1350-1358, Aug. 1994.

[24] C. Du, A. Sannino, and M. H. J. Bollen, "Analysis of the control algorithms of voltage-source converter HVDC," *2005 IEEE Russia Power Tech*, pp. 1-7, 2005.

[25] Y. Liu and Z. Chen, "A flexible power control method of VSC-HVDC link for the enhancement of effective short-circuit ratio in a hybrid multi-infeed HVDC system," *IEEE Trans. Power Syst.*, Vol. 28, No. 2, pp. 1568-1581, May 2013.

[26] C. Liu, C. Liu, R. Shan, Y. Wang, Z. Pei, and H. Ying, "High-frequency-link isolated modular multilevel converter (I-M2C) topology," *2018 IEEE International Power Electronics and Application Conference and Exposition*, pp. 1-6, 2018.

[27] S. Xu, J. Wang, and J. Xu, "A current decoupling parallel control strategy of single-phase inverter with voltage and current dual closed-loop feedback," *IEEE Trans. Ind. Electron.*, Vol. 60, No. 4, pp. 1306-1313, Apr. 2013.

[28] C. Du, M. H. J. Bollen, E. Agneholm, and A. Sannino, "A new control strategy of a VSC–HVDC system for high-quality supply of industrial plants," *IEEE Trans. Power Del*, Vol. 22, No. 4, pp. 2386-2394, Oct. 2007.

[29] S. Burton, C. F. Fuchshuber, D. A. Woodford, and A. M. Gole, "Prediction of core saturation instability at an HVDC converter," *IEEE Trans. Power Del.*, Vol. 11, No. 4, pp. 1961-1969, Oct. 1996.

Ruoshui Zhan received his B.S. degree in Electrical Engineering and Automation from Hunan Institute of Engineering, Xiangtan, China, in 2016. He is presently working towards his M.S. degree at the Changsha University of Technology, Changsha, China. His current research interests include power electronic applications in power systems.

Yanhui Xi received her B.S. and M.S. degrees in Electrical and Information Engineering from Hunan Normal University, Changsha, China, in 2002 and 2005, respectively. She received her Ph.D. degree from Central South University, Changsha, China, in 2013. Her current research interests include traveling identification and signal processing.

Xin Tang received his M.S. and Ph.D. degrees in Control Engineering from the Central South University, Changsha, China, in 2001 and 2005, respectively. He is presently working as a Professor in the Department of Electrical Engineering, Changsha University of Science and Technology, Changsha, China. His current research interests include power electronic applications in power systems and DSP-based control systems.

Xianyong Xu received his B.S. degree in Electrical and Information Engineering and his Ph.D. degree from Hunan University, Changsha, China, in 2005 and 2010, respectively. In June 2010 he started working as an Assistant Engineer and in 2012 he became a Senior Engineer with the Electric Power Corporation Research Institute, Hunan Electric Power Company, Changsha, China. His current research interests include harmonic suppression and reactive power compensation for power electronic devices and active power filters, power quality of microgrids, ultrahigh-voltage ac test systems and their application to UHV ac devices, and electric power saving.